Nayane Macedo Portela da Silva[1]
Jean-Jacques Letourneau[1]
Fabienne Espitalier[1]
Laurent Prat[2]

[1]Université de Toulouse, Mines-Albi, Albi, France.

[2]Université de Toulouse, Institut National Polytechnique de Toulouse, Laboratoire de Génie Chimique, Toulouse, France.

Transparent and Inexpensive Microfluidic Device for Two-Phase Flow Systems with High-Pressure Performance

A design strategy allowing the development of an inexpensive microdevice with a cylindrical section able to work at high pressures is established. The setup combines good optical access, high-pressure resistance, homogeneous operation conditions, fast process control and detection, and the ability to generate a stable two-phase flow. The experiments are conducted in the ionic liquid 1-butyl-3-methylimidazolium hexafluorophosphate and supercritical carbon dioxide flow under isothermal conditions. The two-phase flow system is observed with a high-speed camera. An image processing procedure is performed on the films in order to determine the global two-phase flow geometrical characterizations.

Keywords: High-pressure performance, Ionic liquid, Microdevice, Supercritical CO_2, Two-phase flow

1 Introduction

Microprocess technology is a useful tool that opens new pathways for the development of economical, innovative, and intensified processes. The design of small high-performance devices enables safe, cheaper, compact, sustainable, and energy-efficient technologies. Microdevices include the ability to control the features to the nanometer or micrometer scale, and high throughput is possible with some micro- and nanofabrication methods [1]. This technology plays an increasingly important role in research and development because of its decisive advantages over conventional macroscale technology. For example, the intrinsic small volume allows the use of expensive or toxic chemicals without necessitating large inventory and processing volumes, saving money and time. The large surface area-to-volume ratio offers enhanced heat and mass transfer compared to conventional reactors. Moreover, efficient mixing is a key advantage when materials and/or processes are inhibited by lengthy diffusion time [1, 2].

An additional advantage of the small length scale is the potential for high-pressure applications due to lower mechanical stress in the microdevice material. Therefore, no excessive wall thickness is needed for mechanical stability and the impact of hazardous failure is drastically reduced since only little quantities of materials are involved. Thus, high-pressure microdevices enrich the synthesis spaces and enable supercritical fluid (SFC) applications [3–5].

SCFs exhibit liquid-like densities, allowing dissolution of many organic compounds, and gas-like viscosities and diffusivities, presenting an excellent miscibility with other gases. The main advantage of using SCFs stems from the fact that they can replace many environmentally harmful solvents currently used in industry. Supercritical carbon dioxide is particularly interesting due to its abundance, low cost, and nontoxicity [6–8]. In supercritical fluid process technology, high pressure is the basic requirement. This means a powerful, specialized, and expensive apparatus capable of withstanding the pressure. Usually, such apparatuses offer a restricted access to the interior of the processes, and restriction to perform fast screening for optimization of synthesis conditions [9–11].

Microdevices for high-pressure applications encompass the microfluidic advantages with high-pressure operation performance. These apparatuses are made of different substrates. Silicon/glass microreactors are fabricated using standard photolithography, dry etching, and anodic bonding technique. This technique is applied for catalyzed hydrogenation [3, 12], synthesis of nanomaterials [13, 14], oxidation processes [15], and supercritical extraction of vanillin [16] and lignin oxidation products [17]. Glass microreactors chips are made by means of wet chemical etching [9] or by Pd-immobilized microchannel method [8]. The former was applied to study the formation of benzylmethylcarbamic acid and the latter for hydrogenation reactions using supercritical carbon dioxide as a solvent. Capillary microfluidic technology is also used for high-pressure applications. A quartz capillary microreactor has been devel-

Correspondence: Nayane Macedo Portela da Silva (Nayane.Macedoportela@mines-albi.fr), Université de Toulouse, Mines-Albi, UMR-CNRS 5302, Centre RAPSODEE, Campus Jarlard, 81013 Albi Cedex 09, France.

oped for studies of oxidation in water [11], fused-silica capillary tubing for investigation into multiphase systems [10, 18] and chemical reaction kinetics [19].

One of the main difficulties in manufacturing high-pressure microdevices is to implement mechanically stable microfluidic connections working under desired conditions in terms of temperature, pressure, and flow rates, without breaking the system [3, 5, 9]. The instabilities arise when fragile and different materials with different coefficients of thermal expansion are involved.

So far, there exists no work based on microcapillary technology that describes the design or fabrication methodology applied for high-pressure applications. Furthermore, the macro-to-micro interface by microfluidic interconnectors using this kind of technology has also not been detailed. The design of an inexpensive high-pressure microdevice up to 30 MPa based on capillary microfluidic technology is presented. The strategies applied here overcome the restricted optical access and the instabilities brought by microfluidic connections at high pressure. Hence, this device can be used for optical measurements of two-phase flow at high pressure. The microfluidic setup provides an easy way to investigate two-phase flow systems with a flexible, maintainable, and easy-to-operate platform.

2 Coaxial Microdevice Fabrication

2.1 Materials

A poly(methyl methacrylate) (PMMA) plate purchased from ABAQUEPLAST, France, with dimensions 250×100×15 mm is used. PMMA is a transparent thermoplastic that ensures an excellent transparency and has potential applications in optical devices [4].

Two types of fused-silica capillary tubing (Polymicro, USA) are employed and disposed in a coaxial configuration. The inner capillary is cylindrical with an inner diameter (*ID*) of 100 ± 4 µm and an outer diameter (*OD*) of 363 ± 10 µm. The outer capillary is also cylindrical with an *ID* of 536 ± 6 µm and an *OD* of 665 ± 15 µm. The outer capillary is also cylindrical with an *ID* of 536 ± 6 µm and an *OD* of 665 ± 15 µm. The fused-silica capillaries are coated on the outside with a protective polyimide cladding to protect the fiber from environmental conditions, especially moisture and abrasion, and to reduce the risk of breaking.

The selected optically clear epoxy resin (EP 601-LV, POLYTEC, France) is transparent, optically clear, designed for applications in optics, fiber optics, with excellent adhesion to PMMA. It also presents mechanical properties with die shear strength of 80 N mm^{-2}. The two resin components are mixed in the precise ratio given in the manufacturer's instructions.

Two stainless-steel unions and one stainless-steel tee (Upchurch Scientific, USA) are used with three stainless-steel tubes of 180, 150, and 100 mm in length (*OD* 1.59 mm (1/16″ tubing), *ID* 0.6 mm).

2.2 Fabrication Steps

Design and construction of the microdevice for high-pressure applications is based on capillary microfluidic technology. The chassis manufacturing is the first processing step of microdevice fabrication. The chassis is designed in order to receive all the components of a microsystem and one part is previously configured to the outer silica capillary positioning (Fig. 1 a). This PMMA component is manufactured in a 3D milling machine (Charly 4U CNR3) with oil lubrication.

Once the chassis is ready, the outer capillary cut into 1 m in length is fixed on it with precise alignment. For that purpose, two PMMA plates with dimensions 80×10×2 mm are mounted on the chassis. Tubing sleeves (F-185x, *ID* 395 µm, Upchurch Scientific) of 10 mm in length are placed on the chassis configuration destined to the outer capillary positioning (Fig. 1 b). This technique avoids applying any kind of glue on the system and reduces reaction possibilities with the epoxy resin during annealing.

One side of the outer capillary is connected to the stainless-steel union by means of tubing sleeve with an *ID* of 685 µm. The other side receives the inner capillary configuration (Fig. 1 c).

For the inner capillary configuration, 105 mm in length of the fiber is inserted to the stainless-steel tee and connected to it

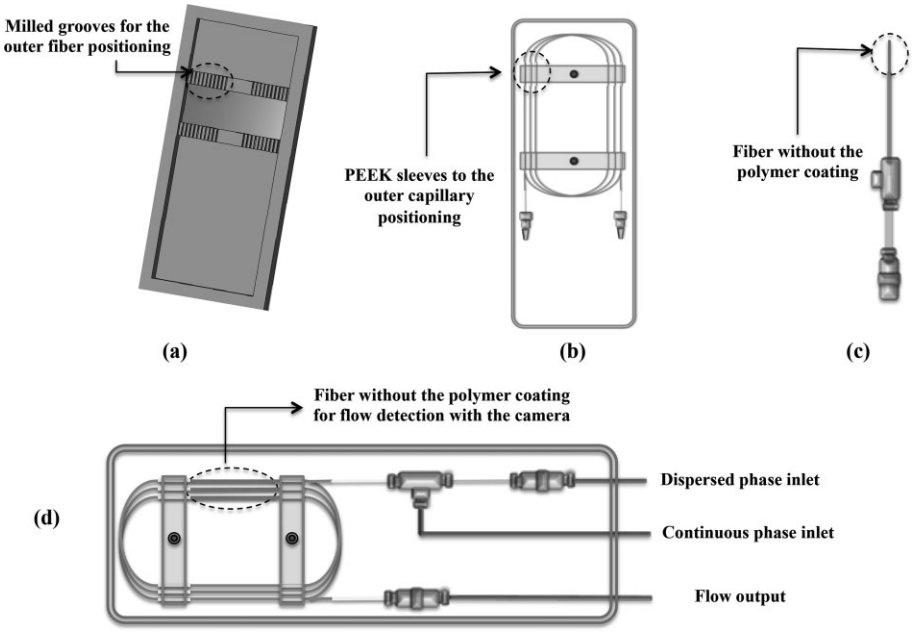

Figure 1. Fabrication steps: (a) PMMA chassis design; (b) outer capillary fixed on the chassis; (c) inner capillary configuration; (d) final microdevice configuration.

by means of tubing sleeve (395 µm, Upchurch Scientific). One end is attached to the stainless-steel union and 10 mm in length of the polymer coating is removed from the fiber to improve optical transparency. The careful removal procedure is done by repeatedly exposing the fiber to the flame for a very short time interval. The residual ashes are removed by means of a paintbrush dip into water. Finally, the final inner capillary configuration is fitted centrally into the outer capillary. The inner capillary configuration is connected with a corrected alignment into the outer capillary from the observation of its position by means of a microscope. The position is adjusted micrometrically in order to obtain a central position into the outer capillary. The resin application step ensures a fixed and central position of the inner capillary.

For the final assemblies, the stainless tubes are connected to the stainless-steel connections. The stainless-steel tube of 150 mm in length is connected to the stainless-steel union from the inner capillary configuration. This allows the entrance of the dispersed phase. The stainless tube of 180 mm in length is attached to the stainless-steel tee for the entrance of the continuous phase. The smallest stainless tube is connected to the stainless-steel union for the flow output. The main limiting factor to perform high-pressure technology using small-diameter tubing is providing connection between the microelements of the device and the macro environmental components [20]. The technique reported in this paper uses integrated connections, i.e., they are directly interconnected to the microfluidic device and overcome the above-mentioned disadvantage.

Once all the microdevice elements have been placed on the chassis, the polymer coating from the outer capillary is removed at the camera detection position. For that, the same methodology described above is applied. The capillaries are used as received and the inner surface remains untreated.

A cleaning procedure is employed before applying the epoxy resin to the device. This step consists of immersion of microcomponents into a flask containing ethanol after assembling. This flask is placed into an ultrasonic bath (Elmasonic X-TRA) at a frequency of 35 kHz at room temperature for 30 min. Excess ethanol is removed and the components are dried in an oven at 343 K (70 °C) for 24 h. This cleaning procedure is implemented to further reduce the influence of contaminants, i.e., organic residues, which are responsible for the appearance of voids or bubbles on the interface during the resin curing time [9].

The last fabrication step is the resin application over the assembled microcomponent device. A capillary without outside polyimide protection is a very fragile and vulnerable system. The resin operation step gives the resistance required for a high-pressure microdevice. The mixture is degassed in a desiccator connected to a pump operating at 40 kPa (400 mbar) at room temperature for 30 min. This operating pressure was chosen because the resin solvent could evaporate under lower pressures. The chassis with all assembled microdevice elements is filled with the degassed resin and then placed in an oven at 308 K (35 °C). The microdevice is ready after 24 h of curing time.

2.3 Advantages of the Microdevice

From the techniques described above, it is possible to acquire microcomponents aligned to the microdevice with a minimum use of tools and leak-free connections under standard operating conditions. The microdevice configuration operates over a range of flow rates, temperatures, and pressures that should be conducted optically, allowing for data detection with a high-speed camera. Therefore, the microdevice fabrication technique presented here fulfils almost all the criteria required to incorporate a successful macro-to-micro interface design [20].

The microdevice described in this paper has the further advantage of a circular cross section compared to the square cross section presented by on-chip microsystems. In fact, the resulting axial symmetry of the flow has both the advantage to drastically simplify CFD simulation and to allow efficient and reliable measurements with image acquisition. This simple and low-cost design strategy is very general and can be applied to a large combination of channel geometries and lengths. The design strategy presented enables to set up microdevices as long as 3 m. Moreover, the chassis configuration can be easily modified to enable devices of 10 m capillary length or more.

In order to compact their total channel length, the 2D design of on-chip based microdevices presents a very small radius of curvature. Due to the 3D design path of capillary-based microdevices, the minimal radius of curvature of the presented configuration is 3 cm and has to be compared to the 100–500 µm radius of curvature of the on-chip 2D design. As long as the two phases are liquids with close density values, a small curvature radius does not present any difficulty. With gas-liquid or supercritical liquid systems for which the fluid density difference is greater, the curvature effect can lead to flow instabilities or to coalescence of the dispersed phase and can even be used to separate phases [21]. These effects could be explained with the help of the Bond (*Bo*) number, which has to be smaller than 1 to avoid such effects. The Bond number compares the body force, i.e., usually the gravity, to interfacial tension forces. In the case of a small radius of curvature, the centrifugal acceleration must replace the gravity acceleration when its value is smaller: $Bo = \Delta\rho a_c L^2/\sigma$[1)], where $\Delta\rho$ is the difference in fluid densities, a_c is the centrifugal acceleration (V^2/R_{curv}), V denotes the flow velocity, R_{curv} the radius of curvature, and L a characteristic length scale. Considering identical mixtures, with identical operating conditions and with the same channel surface sections, the Bond number of the on-chip microdevices (R_{curv} = 0.3 mm) is 100 times higher than of the presented device (R_{curv} = 30 mm).

3 High-Pressure Setup

The microdevice is integrated into a high-pressure experimental setup in order to operate and generate a stable two-phase flow. This apparatus depicted in Fig. 2 allows a maximum operating pressure of 30 MPa. The setup permits an individual

1) List of symbols at the end of the paper.

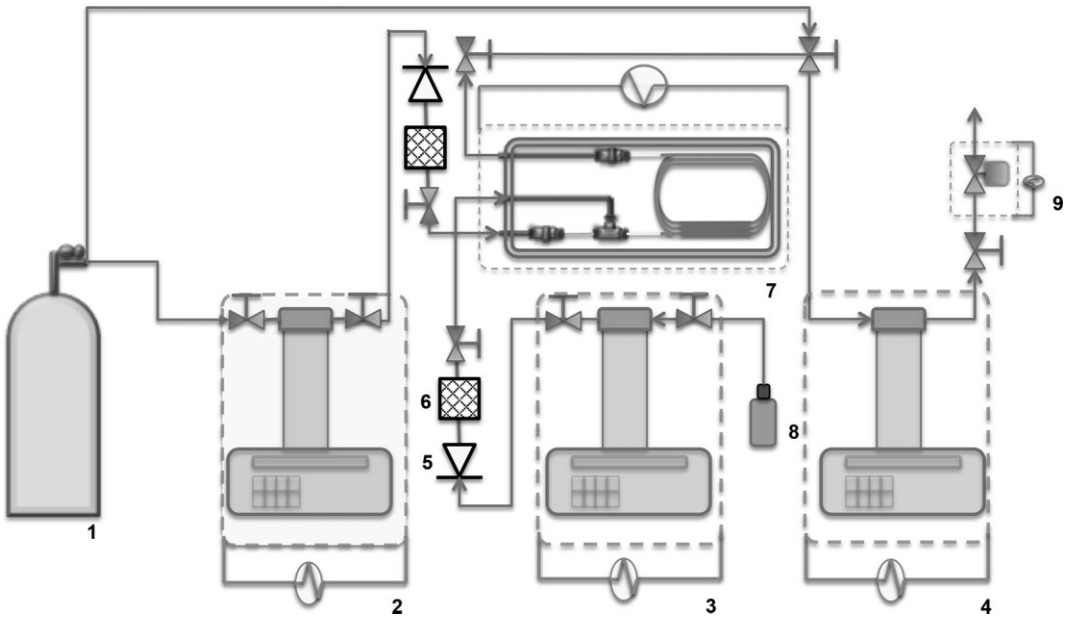

Figure 2. Schematic view of the setup used for the two-phase flow system in a high-pressure capillary microdevice: (1) CO_2 gas tank; (2) high-pressure syringe pump for CO_2 delivery; (3) high-pressure syringe pump for ionic liquid delivery; (4) high-pressure syringe pump for pressure system control; (5) check valve; (6) sintered filter; (7) microdevice; (8) ionic liquid feed solution; (9) back pressure regulator.

adjustment of continuous and dispersed flow rates and the system pressure.

The phase behavior of CO_2 and 1-*n*-butyl-3-methylimidazolium hexafluorophosphate ([bmim][PF_6]) indicates that it is a very unusual biphasic system. Previous work [22] indicates that when CO_2 dissolves in the [bmim][PF_6] (heavy phase), its volume does not change and consequently its density increases. On the other hand, no measurable amount of [bmim][PF_6] transfers in the CO_2-rich phase. These characteristics were a crucial aspect for the binary choice because our microsystem apparatus allows the visualization of changes in properties along the flow path length (Fig. 3).

The continuous phase consists of ([bmim][PF_6]) ionic liquid (99.9 %; Solvionic, France) and the dispersed phase involves CO_2 (purity 99.995 %; Air Liquide, France). Two independent water-cooled high-pressure syringe pumps (ISCO 100 HLX and ISCO 260D) are used for pressurization and conveying of the fluids. The pumps are connected to the microdevice apparatus using stainless-steel tubing fitting by the high-pressure port-connectors. These pumps continuously inject the ionic liquid and CO_2, respectively, into the microdevice at the de-

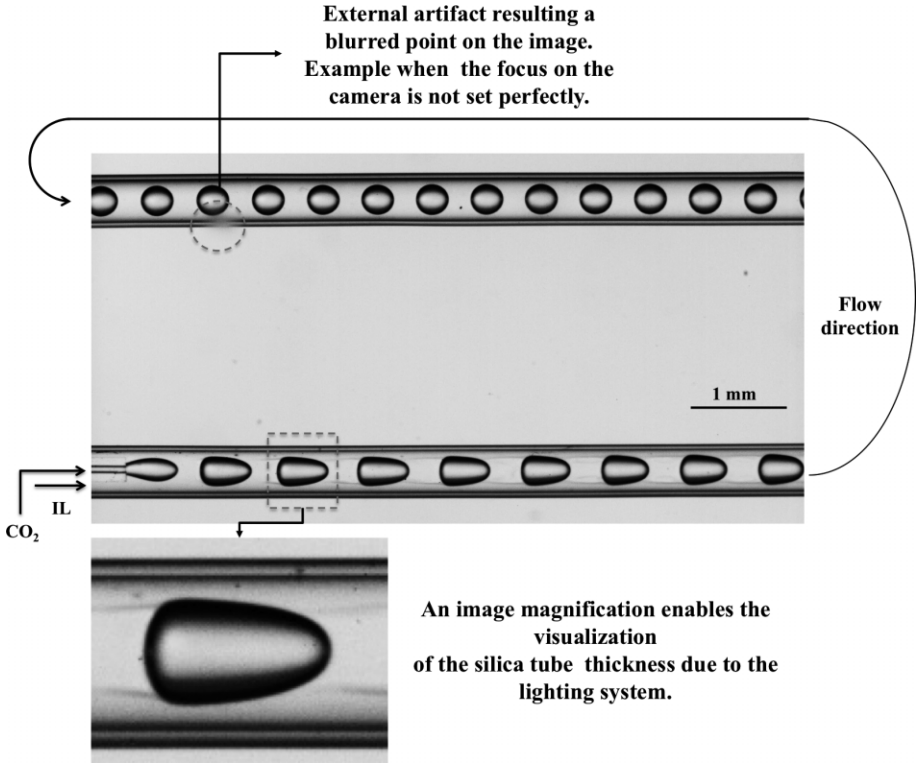

Figure 3. Image of the two-phase flow encountered during experiments showing changes in flow characteristics along its path length. The optical system is chosen to lead an automatic treatment of storage images.

sired system temperature and pressure. The ranges of supercritical CO_2 and ionic liquid flow rates are 1.17–2.17 nm^3s^{-1} (70–130 $\mu L\,min^{-1}$) and 1.17–3.83 nm^3s^{-1} (70–230 $\mu L\,min^{-1}$).

Stainless-steel tubing (*OD* 1.59 mm, *ID* 0.6 mm), high-pressure hand valves, and high-pressure interconnections are used for fluid distribution. At the entrance of the microdevice, the fluids meet at the coaxial outlet configuration, generating a segmented flow into the microdevice.

A safety system is implemented in order to prevent a possible clogging, contamination, and backflow. For this purpose, a check valve and a sintered inline filter with a pore diameter of 0.5 µm are installed before each pump line. The first valve is installed just after the pumps and allows flow in one direction and prevents flow in the reverse direction. At high pressure, the poppet is forced onto the seat hydraulically providing a good seal. The stainless-steel tubing upstream of the check valves is positioned in a way to avoid a liquid accumulation before the ionic liquid pump, preventing backflow. In this configuration, gravity helps the check valve to work. The T-shaped filter is installed downstream of the check valve to reduce risk of clogging or contamination due to impurities.

The microdevice is immersed in a water bath that is made in-house to control the temperature. The pressure inside the microfluidic system is controlled by a third independent water-cooled high-pressure syringe pump (ISCO 260D) running at a constant pressure. A temperature-controlled back-pressure is positioned after the third pump preventing freezing of the valve during the pump depressurization. A flask is placed at the end of the setup line for ionic liquid recuperation. The ionic liquid is degassed in a vacuum oven (Heraeus Vacutherm VT-6025) operating at 2 kPa and at 378 K (105 °C) for 24 h. The depressurization completely removes CO_2 from the ionic liquid phase [22].

4 Optical System

The microdevice placed into the water bath for temperature control is illuminated with LED lamps with a total light intensity of 2200 lumen. The detailed formation of the flow is registered by a CCD camera (Baumer HXC13) with a resolution of 1280×1021 $pixels^2$. The videos can be acquired at 2000 frames per second. Macro camera lens and extension tube were inserted in order to obtain macrophotography with reproduction ratios greater than 1:1.

The distance between the camera lens and the subject, i.e., the image inside the capillary, the field of view and the image resolution are linked. The following parameters are valid: (i) The distance between the camera lens and the capillary plan detection is 120 mm. This configuration produces a clear image only inside the capillary. (ii) The field of view is 8×6 mm^2. (iii) The image resolution (*IR*) is about 6 µm per pixel. These parameters should be well adapted to avoid, e.g., barrel distortion.

For an automatic image treatment, the lighting must be uniform throughout the field of view. LED lamps, or more specifically white LEDs, are a good choice to adapt a powerful and cold lighting system. In the current configuration, the field of view receives 30 % of the light power from the six LEDs installed. These LEDs were disposed on a concave surface to improve the light distribution over the field of view (Fig. 4). This procedure eliminates almost all the optical effects related to the interface contours like boundary thickening or darkness in the picture between the phases or between the fluid and the capillary. The distance between the light source and the capillary should also be adapted to avoid vignetting effects.

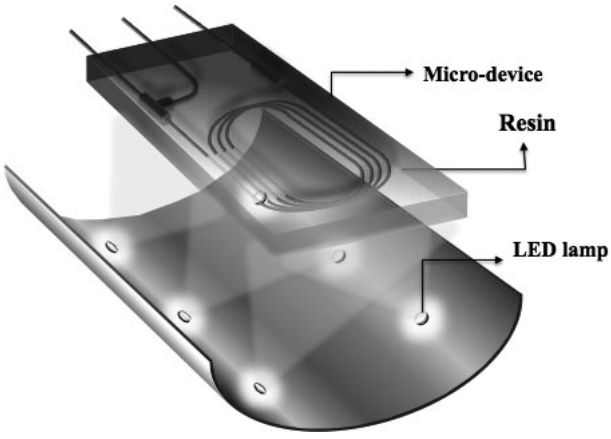

Figure 4. LEDs disposed on a concave surface.

The exposure time (*ET*) can be estimated as a function of bubble rise velocity (*V*) and not as a function of the light intensity. This procedure is established in order to obtain a well-defined sharp picture and to avoid motion blur. For this purpose, the maximal displacement of the bubble (*MDD*) should be equal to 0.5 pixel during image capture. The exposure time can be estimated as follows:

$$ET = \frac{MMD(\text{pixel}) \times IR\ (\text{m pixel}^{-1})}{V\ (\text{m s}^{-1})} \tag{1}$$

The maximum bubble rise velocity observed was 50 $mm\,s^{-1}$. Therefore, the exposure time should be lower than 60 µs.

The depth of field is also an important parameter that could be regulated to eliminate, e.g., external blurred artefacts above or below the image. This parameter can be adjusted to the focal length (*f* number). Here, this value is equal to *f*/2.4 to obtain a clear image only over the capillary plan. The set of all these mentioned parameters could contribute to obtaining good-quality images for an automatic image processing.

5 Image Processing

A software µcap2phase, has been developed to calculate all geometric parameters required for a two-phase periodic flow, i.e., bubble or slug flow. The stored images are further processed in order to calculate the continuous and dispersed phases and unit cell lengths, bubble rise velocity, volume, and area. This software uses routines issued from Image Processing Toolbox of Matlab. The sequence is described below (Fig. 5):

1. A rectangular region of interest that contains part of the capillary is selected and all frames are cropped. The mean image is obtained from the sum of all these gray images. This procedure allows for detecting the inner and outer edge of the capillary. Edge detection is performed using the Canny algorithm. If the camera lens is well adapted to the experimental setup, these edges are straight lines whose dimensions permit to calibrate the images and to straighten up all the sequence. This is effectuated by the slope angles between the frames and the edge straight lines.
2. The capillary boundaries are removed and the internal area, i.e., the two-phase flow, is extracted for all image sequences. Then, the gaps between the bubbles and the capillary inner surface are exaggerated by means of filtering and arithmetical operations in order to help the threshold of the image.
3. Other morphological operations like opening and closing are performed on all threshold images to clean the image. The convex hull of each bubble determines the concave boundary of the dispersed phase. Finally, the geometrical parameters listed above are calculated.
4. The front and rear positions of each bubble as well as its center are detected using the Extrema statistical information implemented by the Region-Props command from Matlab.

Fig. 6 illustrates the continuous and dispersed phases as well as the unit cell lengths. The Guldin-Pappus theorems are used in order to calculate the volume and area of the dispersed phase from 2D information obtained by flow visualization. The method could be applied because this is a cylindrical capillary case and the bubbles present an axisymmetrical profile [23, 24].

The bubble rise velocity was determined from the movies by registering the time required for a bubble to rise a known distance between two images. Under each operational condition, a sequence of at least 1000 images was analyzed and the resulting bubble velocity data were obtained by curve fitting, giving an average value and deviation along the capillary. The stored images that were processed could imply about 50 bubbles that pass over one fixed point of the capillary from a set of parameters, i.e., temperature, pressure, and flow rate, which affects directly the quality and reliability of statistical data. This software (μcap2phase) allows for calculating and fitting the geometrical properties like volume, surface, apex curvature, unit cell length, and center of mass as well as the bubble rise velocity of 100 000 bubbles within about 30 min.

6 Stable Two-Phase Flow Characteristics

As stated previously, the setup is designed in order to operate and generate a stable two-phase flow under high-pressure conditions. This stability should be demonstrated.

Three syringe pumps measure the pressure in this microsystem. The pump, which is connected to the outlet of the microdevice, controls and maintains a constant pressure under working conditions. The two other syringe pumps feed the microdevice with controlled volumetric rates and record the pressure. The pressure drop along the pure CO_2 feeder tube is less than 10 kPa that is why this pressure is set to be the inlet pressure of the two-phase flow.

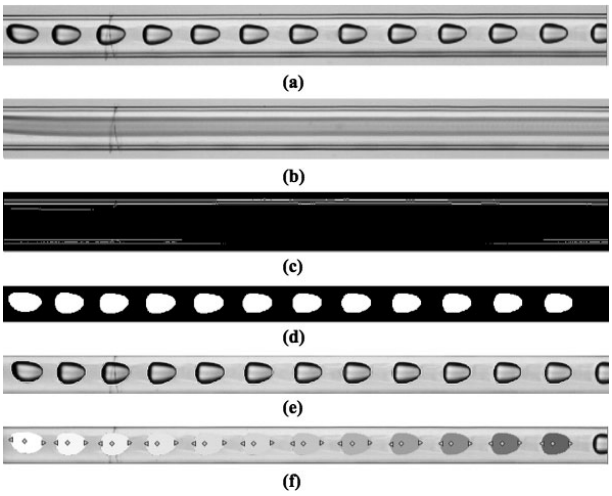

Figure 5. Image processing steps: (a) original crop image. (b) Average frame from the stored images. (c) Edge detection to straighten the final image. (d) Capillary walls subtraction and threshold adjusted image. (e) Edges after finding convex hull, superimposed on the original image. (f) Detection of the boundary points between the phases.

The pressure is measured for different flow rates of both phases versus the time of experiments. The data obtained are presented in Fig. 7. The pressure fluctuations are less than the accuracy measurement of the pump, i.e., 0.01 MPa. As an example, the magnified region in Fig. 7 indicates that there is no change in pressure during acquisition. This behavior confirms the stability of pressure data for the experiments.

The symbol *s* represents the distance of a point along the curvilinear flow path in the capillary from the inlet. The *s*-position of the top, bottom, rear, and front extremities of a bubble are determined using our image processing software μcap2phase. The *s*-positions of the rear extremities of all bub-

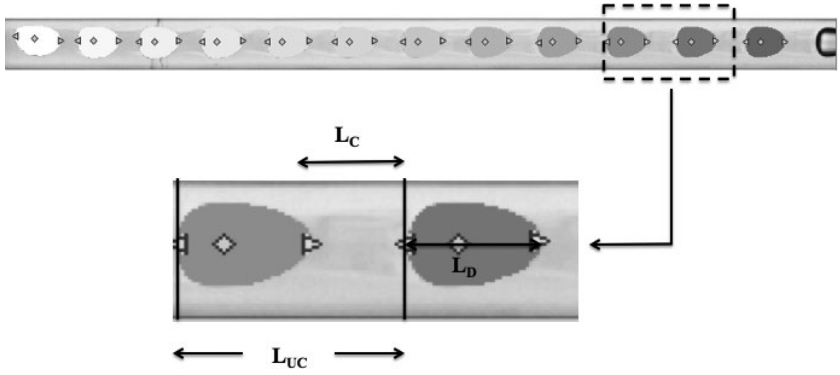

Figure 6. Schematic representation of the two-phase flow global characterizations: length of continuous phase (L_C), length of dispersed phase (L_D), and unit cell length (L_{UC}).

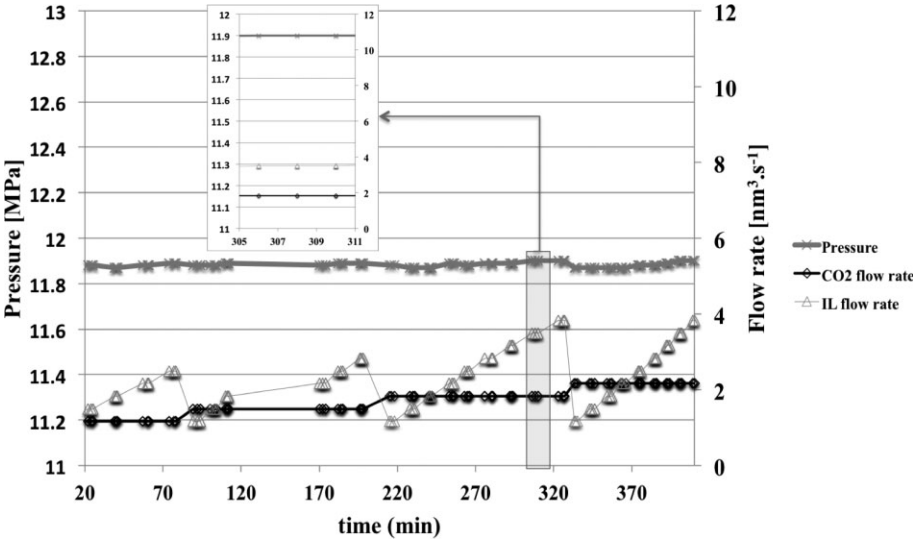

Figure 7. Pressure versus time of experiments for different flow rates of both phases. The detail on the graph shows the pressure data for one set of parameters.

bles are plotted versus time in Fig. 8. The curve slope of each bubble's path gives the velocity, about 0.045 m s^{-1} for this experiment. The slope does not change with time for a given position, confirming the stability of the measurements.

The volume of each bubble is calculated using the 2D surface of the bubble's image and the Guldin theorem. The bubble's volume versus *s*-position is depicted in Fig. 9. The distributions and the mean values of the volume are determined for each *s*-position. These distributions have a deviation, which is the difference between the maximal and the minimal volume at a same *s*-position, of about 0.003 mm^3. In terms of the equivalent radius, i.e., assuming the volumes are spherical, this difference is equal to 8 µm, which is close to the size of a pixel with the image resolution of 7 µm per pixel. One of the advantages of treating all images by the software can be demonstrated here. For one given *s*-position, more than 70 points representing the bubble volumes give a Gaussian distribution that permits to determine the mean value of bubble volumes being 0.022 mm^3 as well its standard deviation of 0.0015 mm^3.

The continuous line represents the mean value of bubble volumes. The volume decreases along the *s*-position. This behavior stems from the particular feature of this binary system, i.e., the CO_2 transfer from the dispersed phase to the continuous phase along the capillary. Furthermore, the volume of the continuous phase does not depend on the quantity of CO_2 transferred.

7 Conclusions

The feasibility of an inexpensive microdevice for high-pressure applications was demonstrated: around 200 € excluding salary costs and investments of the milling machine. The microdevice was fabricated using capillary microfluidic technology with integrated connections. An optically-clear epoxy resin was

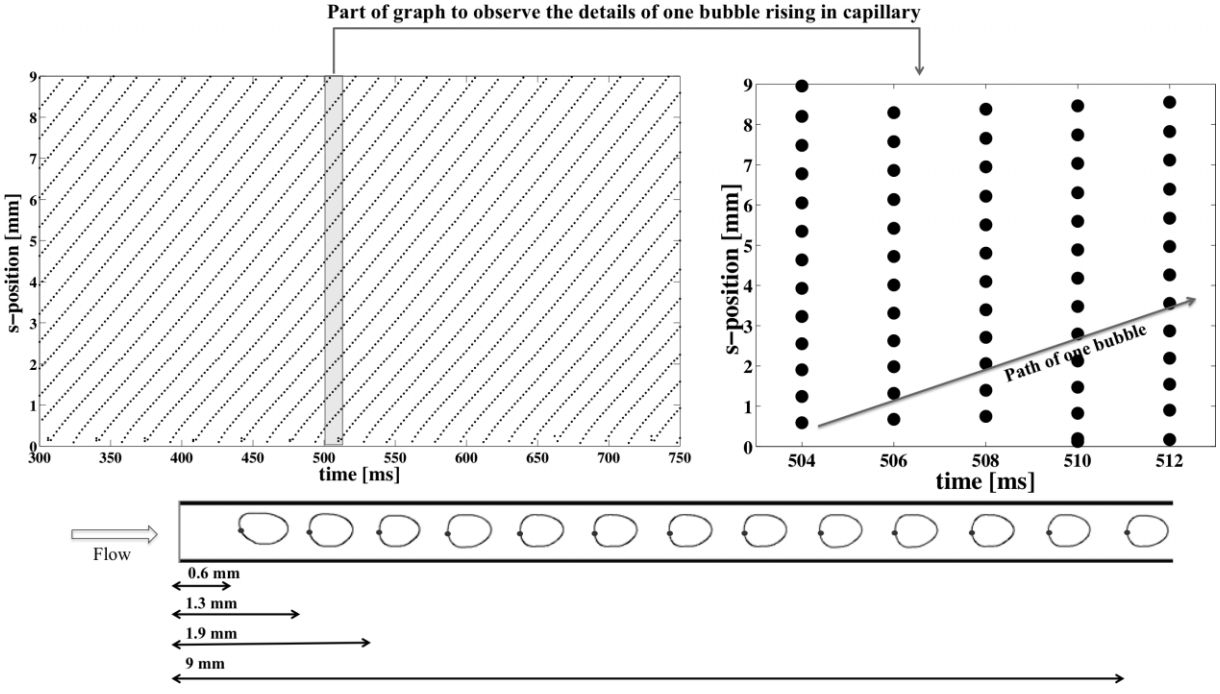

Figure 8. *s*-Position of bubbles versus time. CO_2 flow rate: 1.17 nm^3s^{-1}; IL flow rate: 1.83 nm^3s^{-1}.

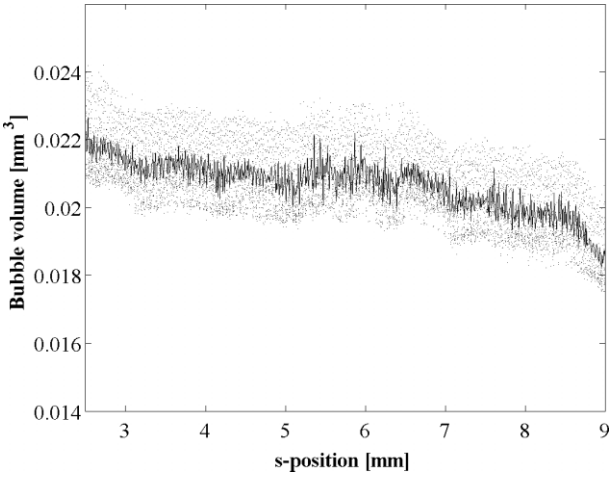

Figure 9. Bubble volumes versus *s*-position.

applied on the microdevice in order to combine optical transparency and mechanical resistance. This microdevice provided a significant reduction in energy density and mass flow rates required to reach supercritical conditions.

Once the microdevice was conceived, an experimental high-pressure setup was designed. Because of the microdevice design, standard instrumentation can be used directly, such as high-pressure syringe pumps, interconnections, hand valves, check valves, and sintered inline filters. The setup was implemented to operate and generate stable two-phase flow and to overcome the difficulties due to restricted optical access, pressure adjustment, and temperature control. Thus, this system enables fast process control and detection and is able to produce homogeneous conditions. Consequently, the described microfluidic high-pressure setup is an optimal configuration for a fast study of processes. The stability of measurements was demonstrated as well.

A high-speed camera was employed for flow visualization and detection. An optical system with an effective focal length of 120 mm and an LED light distribution on a concave surface was implemented. The maximal exposure time should be lower than 60 μs for the bubble rise velocity in the experiments. This combination was employed aiming to avoid external imperfections, which could lead to some limitations on the automatic treatment. The automatic treatment is performed from the visual two-phase flow and the storage images are further processed in a sequence of steps to calculate the global flow characterization. The stability of the two-phase flow system measurements is demonstrated as well. These parameters are crucial to investigate mass transfer from supercritical CO_2 to the ionic liquid in the microdevice.

In future, this study will permit the applicability of high-pressure operations in a simple microcapillary device. In particular, it will enable to investigate the mass transfer of supercritical CO_2 in ionic liquids [25] and to study the particle generation in a two-phase flow system under pressure as well.

Acknowledgment

The authors acknowledge the technical advice of M. Boyer. The authors are also grateful to the Mines Telecom Institute for the financial support of the "Trans-energie" project.

The authors have declared no conflict of interest.

Symbols used

a_c	[m s^{-2}]	centrifugal acceleration
ET	[s^{-1}]	exposure time
f	[–]	*f* number
ID	[μm]	inner diameter
IR	[m pixel^{-1}]	image resolution
L	[m]	characteristic length
MMD	[pixel]	maximal displacement of the bubble
OD	[μm]	outer diameter
R_{curv}	[m]	radius of curvature
V	[m s^{-1}]	bubble rise velocity

Greek letter

$\Delta\rho$	[kg m^{-3}]	density

References

[1] T. Betancourt, L. Brannon-Peppas, *Int. J. Nanomed.* **2006**, *1 (4)*, 483–495.
[2] C.-X. Zhao, L. He, S. Z. Qiao, A. P. Middelberg, *Chem. Eng. Sci.* **2011**, *66 (7)*, 1463–1479.
[3] F. Trachsel, B. Tidona, S. Desportes, P. R. von Rohr, *J. Supercrit. Fluids* **2009**, *48 (2)*, 146–153.
[4] H. Wang, P. Xu, W. Zhong, L. Shen, Q. Du, *Polym. Degrad. Stab.* **2005**, *87 (2)*, 319–327.
[5] S. Marre, Y. Roig, C. Aymonier, *J. Supercrit. Fluids* **2012**, *66*, 251–264.
[6] J. Mitsutoshi, *J. Soc. Rubber Ind.* **2004**, *77 (8)*, 287–292.
[7] S. P. Nalawade, F. Picchioni, L. Janssen, *Prog. Polym. Sci.* **2006**, *31 (1)*, 19–43.
[8] J. Kobayashi, Y. Mori, S. Kobayashi, *Chem. Commun.* **2005**, *20*, 2567–2568.
[9] R. M. Tiggelaar, F. Benito-Lopez, D. C. Hermes, H. Rathgen, R. J. Egberink, F. G. Mugele, D. N. Reinhoudt, A. van den Berg, W. Verboom, H. J. Gardeniers, *Chem. Eng. J.* **2007**, *131 (1–3)*, 163–170.
[10] S. K. Luther, A. Braeuer, *J. Supercrit. Fluids* **2012**, *65*, 78–86.
[11] S. P. Maharrey, D. R. Miller, *AlChE J.* **2001**, *47 (5)*, 1203–1211.
[12] F. Trachsel, C. Hutter, P. R. von Rohr, *Chem. Eng. J.* **2008**, *135 (1)*, 309–316.
[13] S. Marre, J. Baek, J. Park, M. G. Bawendi, K. F. Jensen, *J. Lab. Autom.* **2009**, *14 (6)*, 367–373.
[14] S. Marre, J. Park, J. Rempel, J. Guan, M. G. Bawendi, K. F. Jensen, *Adv. Mater.* **2008**, *20 (24)*, 4830–4834.

[15] S. Marre, A. Adamo, S. Basak, C. Aymonier, K. F. Jensen, *Ind. Eng. Chem. Res.* **2011**, *50 (2)*, 11310–11320.
[16] N. Assmann, S. Kaiser, P. R. von Rohr, *J. Supercrit. Fluids* **2012**, *67*, 149–154.
[17] N. Assmann, H. Werhan, A. Adosz, P. R. von Rohr, *Chem. Eng. Sci.* **2013**, *99*, 177–183.
[18] S. Marre, C. Aymonier, P. Subra, E. Mignard, *Appl. Phys. Lett.* **2009**, *95 (13)*, 134105–134105.
[19] F. Benito-Lopez, W. Verboom, M. Kakuta, J. H. G. E. Gardeniers, R. J. M. Egberink, E. R. Oosterbroek, A. v. d. Berg, D. N. Reinhoudt, *Chem. Commun.* **2005**, *64 (22)*, 2857–2859.
[20] C. K. Fredrickson, Z. H. Fan, *Lab Chip* **2004**, *4 (6)*, 526–533.
[21] D. H. Yoon, J. B. Ha, Y. K. Bahk, T. Arakawa, S. Shoji, J. S. Go, *Lab Chip* **2009**, *9*, 87–90.
[22] L. A. Blanchard, Z. Gu, J. F. Brennecke, *J. Phys. Chem. B* **2001**, *105 (12)*, 2437–2444.
[23] T. Thulasidas, M. Abraham, R. Cerro, *Chem. Eng. Sci.* **1995**, *50*, 183–199.
[24] M. T. Kreutzer, F. Kapteijn, J. A. Moulijn, J. J. Heiszwolf, *Chem. Eng. Sci.* **2005**, *60 (2)*, 5895–5916.
[25] J.-J. Letourneau, L. Prat, *European Conference on Microfluidics*, Bologna, December **2008**.